AN OPTIMIZED ROOTS POWER MACHINE BASED ON NEGATIVE DISPLACEMENT THEORY

Yanjun XIAO[12*], Jing GAO, Jiamin REN, Wei ZHOU, Feng WAN, Weiling LIU[1*], Yunfeng JIANG[1*]

[1]Department of measurement and control, School of Mechanical Engineering, Hebei University of Technology, Tianjin, China

[2]Jiangsu kered Intelligent Control Automation Technology Co., Ltd, Jiangsu, China

[*] Yanjun Xiao; E-mail: xyj@hebut.edu.cn; Weiling LIU; E-mail: Lwl@hebut.edu.cn; Yunfeng Jiang; E-mail: jyf@hebut.edu.cn

Roots power machine has obvious advantages in low and medium temperature waste heat recovery. The existing roots power machine has the problem of internal flow field disturbance, which seriously affects the power generation efficiency of the power machine. In order to solve the problem of disturbance of the internal flow field of roots power machine, the traditional involute rotor roots power machine is improved, and the roots power machine based on negative displacement involute rotor is proposed. The structure model and turbulence model of roots power machine are constructed, and the internal flow field simulation of roots power machine is realized by computational fluid dynamics. The pressure contour and torque change of roots power machine before and after improvement are compared, and the experimental research on the improved structure is carried out.The results show that the intensity of flow field disturbance in the modified involute rotor roots power machine decreases, and the working performance of the roots power machine improves,which provides a reference for the structural improvement and performance optimization of roots power machine.

Key words*: Roots power machine; Turbulence model; negative displacement involute rotor; flow field disturbance*

1. Introduction

With the rapid development of the world economy, the demand for energy in various countries is growing. The shortage of energy resources has become an important factor restricting economic and social development. The fundamental reason for the severe energy situation lies in the low efficiency of energy use. About 60-65% of industrial energy is converted into waste heat resources. At present, the country with the most waste heat utilization is the United States, whose utilization rate is 60%, that of Europe is 50%, and that of China is only 30%[1]. The utilization rate of waste heat resources has a large space for improvement.

The existing waste heat conversion machinery mainly includes steam turbine, screw expander, scroll expander, roots power machine, etc[2]. Manoj Kumar *et al.* Designed the profile of radial inflow turbine according to different loss models[3]. Sobol sensitivity analysis is used to identify the main

geometric parameters that affect turbine performance. Based on geometric data sets, Ann and ANFIS developed models to predict the maximum efficiency of turbines obtained with minimum energy loss. Sun Yajing et al[4]. Carried out the finite element simulation and Experimental Research on the twin-screw expander. The complexity of the internal flow field of the expander was well illustrated by the velocity streamline and velocity vector diagram of the flow field. Diaoanna et al[5]. Studied the oil-free screw expander, refined the leakage channel model, analyzed and compared the change trend of volume efficiency with meshing clearance, tooth top clearance and end clearance, among which the tooth top clearance had the greatest impact on volume efficiency. Yuan Weiwei analyzed the force and deformation of the screw expander rotor [6]. He proposed a more accurate and reliable calculation method for more reasonable design of rotor clearance by using the fluid structure coupling method.

The roots power machine is an improved application of Roots blower. It can convert the low quality waste heat resource which is difficult to be used by steam turbine into mechanical energy. It has the advantages of simple structure and high utilization rate of heat energy[7]. Kong Xuan proposed that the gradually opening linear blade structure is beneficial to the performance and stability of roots power machine[8]. Wang D.Y. optimized the structure of roots steam power machine and pointed out that the stability of three blade roots power machine is better than that of two blade roots power machine[9]. Cai Yuqiang improved the rotor profile of the involute roots compressor and made dynamic simulation. The internal flow field of the involute roots compressor is more stable[10].

There are many researches on the rotor profile in the existing literature, but the derivation of the rotor profile and the analysis of the internal flow field disturbance caused by the structure change of the profile are not enough[11]. When the steam enters the cavity of the roots motor, due to the different rotor structure, there will be different meshing clearance and different flow field, the flow field will be disturbed to different degrees, and the disturbance intensity will affect the different working characteristics of the roots motor. Through theoretical analysis, structural improvement, software simulation and experimental verification, the influence of different rotor profiles on the working performance of roots motor is studied. It provides a new idea for the tooth profile design and performance optimization of roots power machine.

2. Optimization of rotor profile

The theory of negative displacement was originally applied to the machining of involute gear. In some places of mechanical transmission, the modified gear is often used. On the one hand, the traditional involute rotor structure will make the rotor trapped in the middle of the meshing position, which is not conducive to the stability of the rotor operation, and cause the internal flow field disturbance. On the other hand, the rotor will expand in the high temperature operation environment, further reducing the meshing clearance between the rotors, and even interference. Therefore, the design method of negative displacement rotor profile is proposed[12]. The rotor of roots power machine adopts the profile of negative displacement involute rotor, which can effectively solve the wear problem of rotor caused by high temperature expansion, increase the engagement degree of rotor, and improve the stability of roots power machine operation.

2.1. Construction of negative displacement rotor profile

As shown in Fig. 1, select a pair of rotors for analysis and modeling. The rotation centers of left and right rotors are O_1 and O_2 respectively. The outer radius of the rotor is R_1. Shell radius is R_0. The center distance between two rotors is $2a$.Radius of index circle is R_2.Base circle radius is R_3. $\angle A_1O_1C$ is 30 degrees. $\angle AO_1C$ is θ,Radius of tooth top arc is R_5.Radii of dedendum arc is R_6 [13]. The intersection of involutes of left and right rotors is B_1. The clearance between the addendum circle and the dedendum circle is μ. The involute AFB is the involute $A_1F_1B_1$, which is obtained by turning γ anticlockwise.

① Involute $A_1F_1B_1$ equation

$$\begin{cases} x_1 = R_3(\cos\theta + \theta\cdot\sin\theta) \\ y_1 = R_3(\sin\theta - \theta\cdot\cos\theta) \end{cases} \tag{1}$$

② The involute AFB is the involute $A_1F_1B_1$

$$\mu = 2R_3\tan\gamma \tag{2}$$

③ Involute AFB equation

$$\begin{cases} x = R_3(\cos\theta + \theta\cdot\sin\theta)\cos\gamma - R_3(\sin\theta - \theta\cdot\cos\theta)\cdot\sin\gamma \\ y = R_3(\sin\theta - \theta\cdot\cos\theta)\cos\gamma + R_3(\cos\theta + \theta\cdot\sin\theta)\cdot\sin\gamma \end{cases} \tag{3}$$

④ F_1 is the intersection of involute $A_1F_1B_1$ and index circle R_2

$$\begin{cases} x_{F_1} = R_2\cos\theta_{F_1} \\ y_{F_1} = R_2\sin\theta_{F_1} \end{cases}$$
$$\begin{cases} x_{F_1} = R_3(\cos\theta_{F_1} + \theta_{F_1}\cdot\sin\theta_{F_1}) \\ y_{F_1} = R_3(\sin\theta_{F_1} - \theta_{F_1}\cdot\cos\theta_{F_1}) \end{cases} \tag{4}$$

⑤ Line A_4G is tangent of base circle R_3

$$\begin{cases} x_{A_4} = R_3\cos(2\theta_{F_1} + \dfrac{\pi}{3}) \\ y_{A_4} = R_3\sin(2\theta_{F_1} + \dfrac{\pi}{3}) \end{cases}$$
$$\begin{cases} x_G = R_2\cos(\theta_{F_1} + \dfrac{\pi}{6}) \\ y_G = R_2\sin(\theta_{F_1} + \dfrac{\pi}{6}) \end{cases} \tag{5}$$

⑥ The linear equation of A_4G line

$$\frac{x - x_G}{x_{A_4} - x_G} = \frac{y - y_G}{y_{A_4} - y_G} \tag{6}$$

⑦ Point B_1 is the intersection of tangent A_4G and involute $A_1F_1B_1$, point B is the

intersection of tangent A_4G and involute AFB, point B_3 is the intersection of tangent A_1G and involute $A_3F_3B_3$, point C is the intersection of line O_1G and tooth top circle R_1. The tooth top circle arc can be determined, similarly, the tooth root circle arc can be determined.

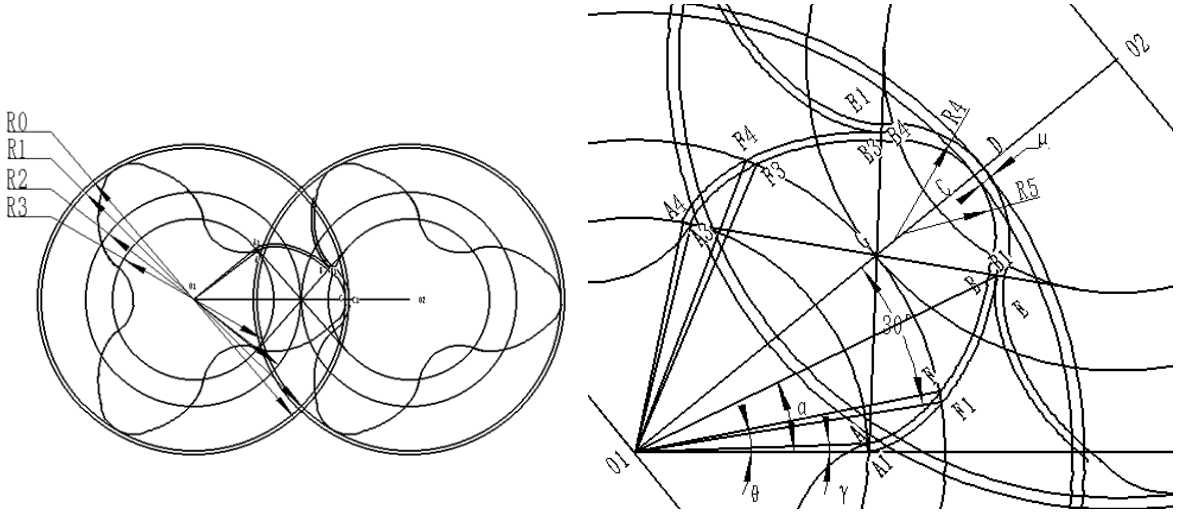

Fig. 1 (a)Engagement diagram of negative displacement rotor (b)partial enlarged diagram of engagement of negative displacement rotor

2.2. Comparative analysis of traditional involute roots rotor and involute negative displacement rotor

Based on the above method, the profile of the improved involute rotor can be obtained according to the change of the base circle size. As shown in Fig. 2.

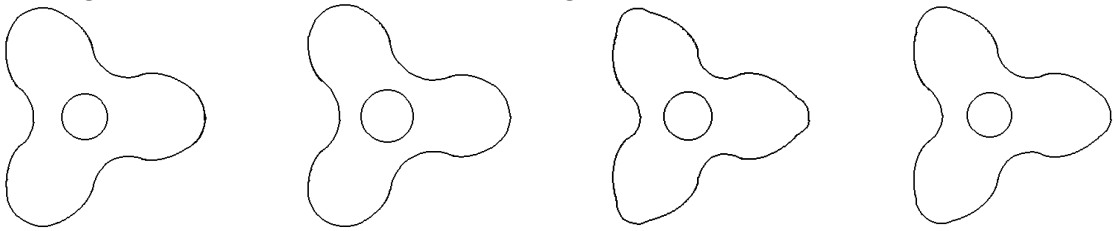

Fig. 2 Improved involute rotor and traditional involute rotor (a)Traditional rotor(b)Base circle 90 involute rotor(c)Base circle 80 involute rotor(d)Base circle 70 involute rotor

Compared with four kinds of involute rotors, the area utilization ratio of three kinds of improved involute rotors is higher than that of traditional involute rotors[14]. Among them, the involute length of the involute rotor with base circle 70 is the longest, and the area utilization coefficient is the largest. The comparison of four rotor parameters is shown in Tab. 1.

Tab. 1 Data comparison between traditional and improved involute rotors

Serial number	Base circle radius R3 / mm	Involute generating line length L/ mm	Area utilization coefficient η
a	83.7153	60.0790	0.4675
b	90	60.1611	0.4967
c	80	78.6603	0.5022
d	70	80.3792	0.5060

3. Simulation of internal flow field

3.1. The establishment of the calculation model of roots power machine

The shell mainly includes air inlet, cavity and exhaust port. The complex structures are ignored to reduce the complexity of the model. The assembly method is shown in Fig. 3.

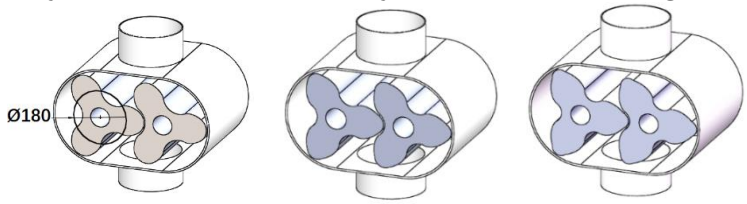

Fig. 3 Assembly diagram of negative displacement involute rotor (a)Base circle 90 involute rotor(b)Base circle 80 involute rotor(c)Base circle 70 involute rotor

3.2. Three-dimensional computational domain grid of roots power machine

Tetrahedral mesh is used in the rotating part to reduce the distortion of the mesh as much as possible to improve the convergence of the calculation[15]. As the Fig. 4 shown, the initial mesh number of the flow field in the base circle 90 roots power machine is 40376. The initial mesh number of the flow field in the base circle 80 roots power machine is 41256. The initial mesh number of the flow field in the base circle 70 roots power machine is 40713.

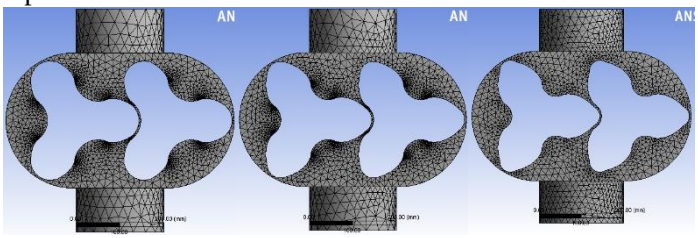

Fig. 4 Mesh generation of flow field model of negative displacement involute rotor roots power machine(a)Base circle 90 rotor(b)Base circle 80 rotor(c)Base circle 70 rotor

3.3. Verification of grid independence

The computational domain of the model includes four sub domains: the intake, the exhaust, the rotating rotor and the working cavity. The mesh quality of each calculation domain of the model should meet the requirements of orthogonality, aspect ratio and distortion, especially to ensure that there is no negative volume mesh in the dynamic calculation domain. Tab. 2 shows grid mass of each sub calculation domain of roots power machine[16].

Tab. 2 Grid mass of each sub calculation domain of roots power machine

Calculation domain name	Grid quality evaluation index and scope		
	Orthogonality	Aspect ratio	Distortion
Inlet	0.781-1	1.798-3.652	0.028-0.429
Exhaust port	0.818-1	1.813-4.357	0.032-0.432
Rotating rotor	0.882-0.999	2.653-3.711	0.002-0.243
Working chamber	0.512-1	3.243-14.876	0.002-0.722

Before the numerical simulation, it is necessary to verify the grid independence of the numerical model, select the appropriate grid scale and number, and improve the calculation efficiency on the premise of ensuring the calculation accuracy[17]. In order to select the appropriate grid scale and number of calculation domain, the numerical calculation results of three different number of grid models under specific conditions are compared, as shown in Tab. 3.

Tab. 3 Time average performance parameters of the different roots power machine with different mesh numbers

Grid level	Total number of grids	rate of flow【kg/s】
Sparse(90)	30321	1.351
Secondary(90)	40376	1.353
Fineness(90)	52137	1.352
Sparse(80)	31821	1.348
Secondary(80)	41256	1.349
Fineness(80)	50217	1.351
Sparse(70)	30193	1.353
Secondary(70)	40713	1.354
Fineness(70)	53179	1.351

Compared with sparse grid and fine grid, the deviation of mass flow of medium grid is less than 0.5%. It can be seen that the numerical simulation of the expander model with a medium number of grids has met the requirements of grid independence and calculation accuracy.

3.4. Turbulence model construction

The internal flow field in the cavity of roots power machine is turbulent motion. The recombined group $RNG\ k-epsilon$ model is mainly aimed at the high Reynolds number flow problem[18]. It is also beneficial to deal with the flow near the wall, and has higher accuracy and reliability in the prediction of strong streamline bending, complex shear flow, rotating flow field and separation flow field.

3.5. Comparative analysis of pressure contour

In the trial calculation, after several attempts, the set time step is determined to be 0.0001s, and after 400 steps of iteration, the periodic change diagram of the pressure contour of roots power machine is obtained[19]. Since the rotor is in periodic circular rotation, take three pressure contours with symbolic angles for observation and analysis. The pressure contour distribution before and after optimization is shown in Figs. 5-8. By observing and comparing the distribution of pressure contour, it can be found that the pressure changes of the two are basically similar, which is generally consistent with the change rule of working mechanism of roots power machine. The red part represents the maximum pressure, and the blue part represents the minimum pressure. The color changes gradually with the change of pressure, which means that the pressure at the inlet is the highest and the pressure at the outlet is lost[20]. However, at the engagement of a pair of rotors and the gap between the rotor and the casing, because the gap is very long and narrow, the pressure changes violently, and this part of color block is also one of the focuses of the comparison between the two.

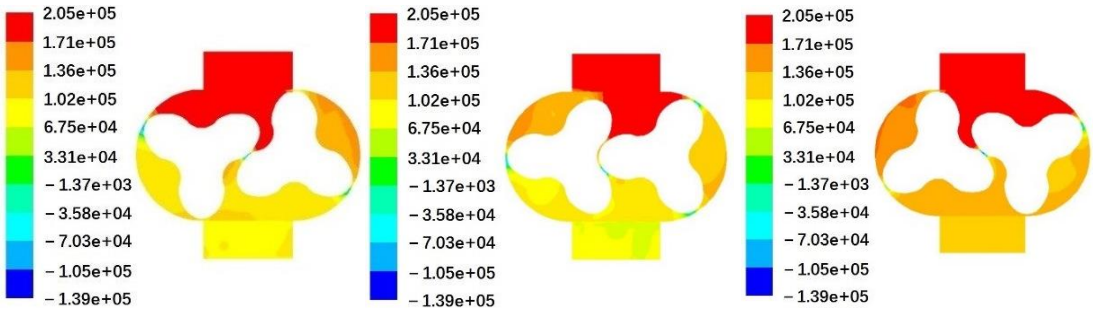

Fig. 5 Pressure contour distribution of conventional involute roots power machine(a) Turn 30 °(b) Turn 60 °(c) Turn 90 °

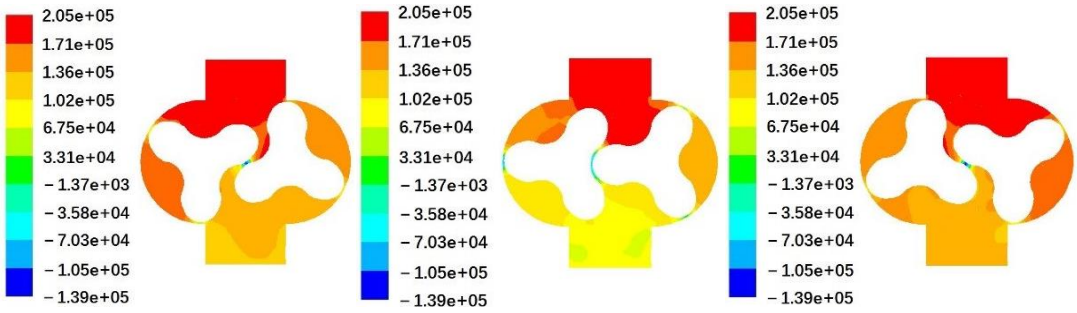

Fig. 6 Pressure contour distribution of roots type power machine with involute base circle 90 (a) Turn 30 °(b) Turn 60 °(c) Turn 90 °

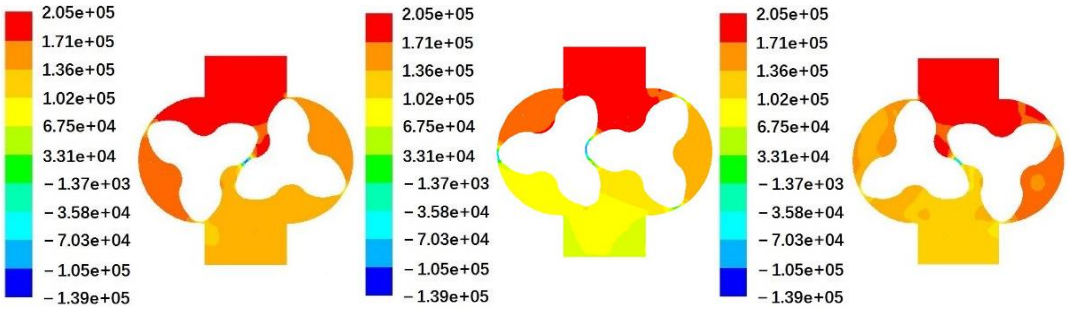

Fig. 7 Pressure contour distribution of roots type power machine with involute base circle 80 (a) Turn 30 °(b) Turn 60 °(c) Turn 90 °

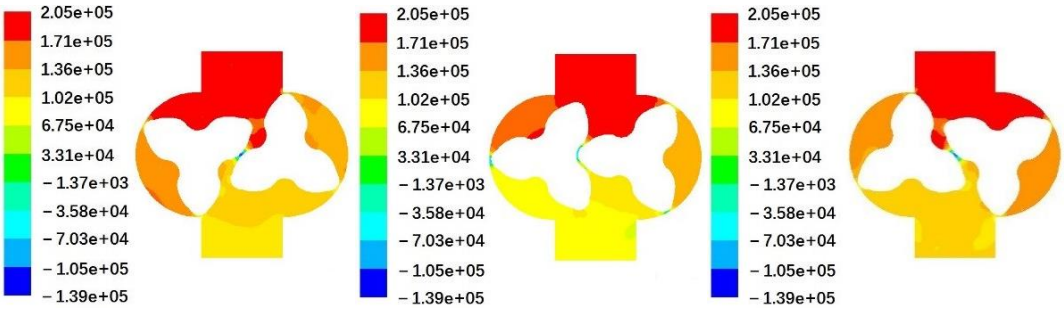

Fig. 8 Pressure contour distribution of roots type power machine with involute base circle 70 (a) Turn 30 °(b) Turn 60 °(c) Turn 90 °

The opening and closing of roots power unit is transient, but the gap between rotor and casing and the gap between rotors are very small, so the high and low pressure alternate at the gap, and the pressure situation is complex. Compared with the pressure map before and after the optimization, the

color overlap before the optimization is more intense, and the high and low pressure overlap after the optimization is more gentle, the higher the alternation of high and low pressure, the stronger the disturbance of internal flow field, the greater the energy loss. Compared with the optimized internal pressure contour distribution of different base circle roots power machine, the pressure at the outlet of base circle 80 and base circle 90 involute roots power machine is large, and the heat energy cannot be fully utilized due to the intense disturbance of the internal flow field of rotor instantaneous base circle closure and opening 30 and 90 degrees. The results show that the 70 base circle rotor has a good effect, and it has a good adaptability to the instantaneous base circle opening and closing of the rotor.

3.6. Comparison of torque coefficient curve of roots power machine

As shown in Fig. 9 ,the torque value directly reflects the dynamic performance of the roots power machine. By comparing the torque performance of the rotors with different base circle sizes, the negative torque of the rotors with base circle 70 is significantly higher than that of the rotors with base circle 80 and 90 in 0.0025s, and the first peak value of the torque is reached near 0.005s. The peak value is basically the same. At 0.01s, the second rotor appears The peak value of the base circle 70 rotor is slightly lower than that of the other two rotors. Near 0.015s, the torque of the base circle 70 rotor roots power machine is higher than that of the other two rotors[21]. It can be seen from the rotor torque chart that the torque performance of the base circle 70 rotor is more stable and the dynamic performance is more superior. At the same time, the analysis of the operating characteristics of the rotor also provides a theoretical basis for the regulation of other key components.

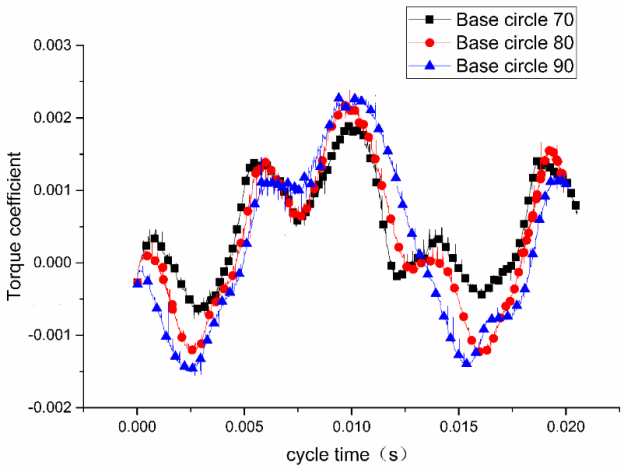

Fig. 9 Torque coefficient curve of different rotors

4. Experiment

4.1. Test platform design

The purpose of this test is to demonstrate whether the power of the power machine before and after optimization can be significantly improved at different rotating speeds under the unstable steam condition. Through comparative analysis of the data before and after optimization, the conclusion before optimization can be verified.

Combined with the analysis and research in the previous chapters, a new prototype is designed and manufactured based on the parameters of the optimized roots power machine, as shown in Fig. 10, and the conventional parameters of the prototype are shown in Tab. 4.

Fig. 10 Negative displacement involute rotor roots power machine

Tab. 4 Structural parameters of roots power machine

Name	Pre optimization value/mm	Optimized value/mm
Size of inlet and outlet	φ200	φ200
Axial length of rotor	355	355
Cavity diameter	304	304
Center distance between two rotors	213	213
Radial clearance between rotor and shell	1.6	2
Rotor shaft diameter	65	65

Due to the poor safety of using low-grade steam working medium, the screw air compressor is used as the power source of the test platform. The test platform of the power generation device includes control pipeline, control valve, three blade twisted blade roots power machine, reducer, coupling, etc., as shown in Fig. 11 . In order to obtain more accurate test data, the flow, pressure and temperature detection instruments are installed at the inlet pipe, and the torque sensor is installed at the outlet pipe. The power machine, torque sensor and generator are coaxially connected by coupling. At the same time, the control system monitors each index and controls the opening of flow valve by timely feedback data.

Fig. 11 Test platform of roots type power generation device

4.2. Result analysis

The most important index to judge the working performance of roots power machine is the output power. The larger the output power of generator is, the higher the conversion efficiency of roots power machine for thermal mechanical energy electric energy is, that is to say, the stronger the generating performance of generator. The actual power of the generator before and after the roots power machine optimization is shown in Fig. 12.

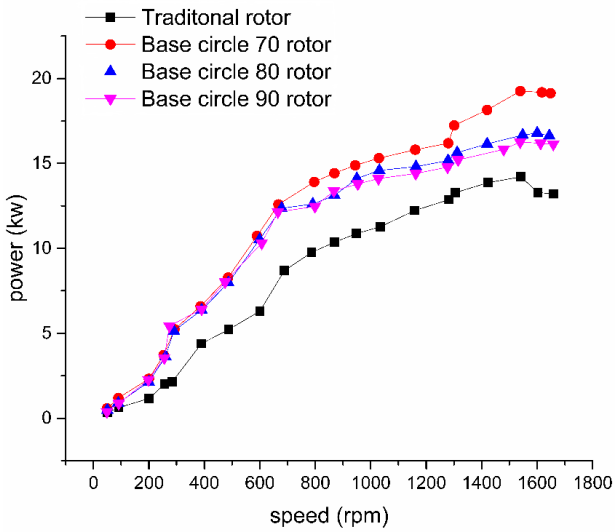

Fig. 12 Power speed comparison curve of power machine before and after optimization

Fig. 12 shows that with the increase of rotating speed, the output power of roots power generation device tends to be parabolic. It increases first and then reaches the peak value and tends to be flat. Under different power, the maximum speed of roots power machine rotor can reach 1621 rpm, which is 231 rpm higher than that before optimization. After optimization, the output power curve is above that before optimization. After optimization, the output power of roots power machine with base circle 70 rotor is the best. Therefore, the output power of roots power machine can be improved by optimizing and increasing the maximum speed.

5. Conclusions

This paper studies the disturbance of the internal flow field of the existing involute roots power machine, puts forward the design method of the negative displacement involute line, builds the structure model of the negative displacement involute rotor, and carries out the unsteady numerical simulation analysis on the platform of Fluent-Ansys, and carries out the experimental research on the modified model. It provides a basis for the performance optimization of roots power machine. According to the data analysis before and after optimization, the following conclusions are drawn:

(1) With the improved negative displacement involute rotor roots power machine, the air transportation between the unit volume and the inlet and outlet is more smooth and stable, the internal flow field disturbance is smaller, the alternation of high and low pressure is smoother, and the working performance is more stable;

(2) In the improved negative displacement involute rotor roots power machine, the torque change of the involute rotor roots power machine with base circle 70 is more stable, which verifies (1) the accuracy of flow field calculation, and infers that the mechanical efficiency of the involute rotor roots

power machine with base circle 70 is better than that of the involute rotor roots power machine with base circle 80 and base circle 90.

(3) The power of the improved negative displacement involute rotor roots power machine is higher than that of the traditional involute rotor roots power machine, and the working performance of the improved roots power machine is better, and the accuracy of (1) (2) conclusion is verified.

Acknowledgment

This work was supported by the fund of Tianjin science and technology program (15JCTPJC62400).

Nomenclature

B_1	Intersection of involutes of left and right rotors	R_0	Shell radius(mm)
O_1	Rotation centers of left rotors	R_1	Outer radius of the rotor(mm)
O_2	Rotation centers of right rotors	R_2	Radius of index circle(mm)
$2a$	Center distance between two rotors(mm)	R_3	Base circle radius(mm)
R_6	Radii of dedendum arc(mm)	R_5	Radius of tooth top arc(mm)
L	Involute generating line length (mm)	η	Area utilization coefficient
μ	Clearance between the addendum circle and the dedendum circle(mm)		

References

[1] Papes, I. *et al.*, Development of a thermodynamic low order model for a Twin Screw Expander with emphasis on pulsations in the inlet pipe, *Applied Thermal Engineering*, 103(2016), pp.909-919.

[2] Zoghi, M. *et al.*, Thermo-economic assessment of a novel trigeneration system based on coupling of organic Rankine cycle and absorption compression cooling and power system for waste heat recovery, *Energy Conversion and Management*, 196 (2019), pp.567-580.

[3] Deng, S. X. *et al.*, Global well posedness of a class of dissipative thermoelastic fluids based on fractal theory and thermal science analysis, *Thermal Science*, 23 (2019), pp.2461-2469.

[4] Qiu, Y. Y, Solving a class of boundary value problems by lsqr, *Thermal Science*, 21(2017), pp.1719-1724.

[5] Chatzopoulou, M. A., *et al.*, Off-design optimisation of organic Rankine cycle (ORC) engines with different heat exchangers and volumetric expanders in waste heat recovery applications, *Applied Energy*, 253(2019),pp.1211-1236.

[6] Zhang, S., and Gao, X. D., Analytical treatment on a new generalized ablowitz-kaup-newell-segur hierar of thermal and fliud equations, *Thermal Science*, 21(2017), pp.1607-1612.

[7] Zheng, S. Q., and Lu, J. F., A relaxed non-linear inexact uzawa algorithm for stokes problem, *Thermal Science*, 23(2019), pp.2323-2331.

[8] Li, Y. Y. *et al.*, Thermodynamic analysis of a novel combined cooling and power system utilizing liquefied natural gas (LNG) cryogenic energy and low-temperature waste heat, *Energy*, 199(2020). 117479

[9] Manjunath, K. *et al.*, Entropy generation and thermoeconomic analysis of printed circuit heat exchanger using different materials for supercritical CO 2 based waste heat recovery, *Materials Today: Proceedings,* 21(2020),pp.1525-1532.

[10] Chen, W. H. *et al.*, A computational fluid dynamics (CFD) approach of thermoelectric generator (TEG) for power generation, *Applied Thermal Engineering,* 173 (2020), 115203.

[11] Imran, M. *et al.*, Volumetric expanders for low grade heat and waste heat recovery applications, *Renewable & Sustainable Energy Reviews,* 57 (2016), pp.1090-1109.

[12] Oluleye, G. *et al.*, Evaluating the potential of process sites for waste heat recovery, *Chemical Engineering Transactions,* 39(2016), pp. 627-646.

[13] Xu, S., *et al.*, Heat transfer performance of a fractal silicon microchannel heat sink subjected to pulsation flow, *International Journal of Heat & Mass Transfer,* 81(2015),pp.33-40.

[14] Arellano, C. *et al.*, Envelope condition method with an application to default risk models, *SSRN Electronic Journal,* 69(2016),pp.436-459.

[15] Cataldo, F. *et al.*, Fluid selection of Organic Rankine Cycle for low-temperature waste heat recovery based on thermal optimization, *Energy*, 72(2014),pp.159-167.

[16] Kong, X. *et al.*, Design and feasibility study of roots-type power machine rotor based on numerical simulation, *Neural Computing & Applications,* 32(2020),pp.223-234.

[17] Wang, D. Y., Research on structural optimization of roots steam power machine, Tianjin: Hebei University of technology, (2016).

[18] Davide, Z. *et al.*, Review and update on the geometry modeling of single-screw machines with emphasis on expanders, *International Journal of Refrigeration,* 92(2018),pp.10-26.

[19] Arellano, C., *et al.*, Envelope condition method with an application to default risk models, *Ssrn Electronic Journal,* 69(2016),pp.436-459.

[20] Wang, Y. *et al.*, LIS-PRO: A new concept of power generation from low temperature heat using liquid-phase ion-stripping-induced salinity gradient, *Energy*, 200(2020), 117593.

[21] Moser, S. *et al.*, Designing the Heat Merit Order to determine the value of industrial waste heat for district heating systems, *Energy*,200(2020), 117579.